Conference on Modelling Fluid Flow (CMFF'22)
The 18th International Conference on Fluid Flow Technologies
Budapest, Hungary, August 30-September 2, 2022

MECHANISTIC TURBULENCE: TARGETED ENERGY TRANSFER IN A MULTI-DEGREE-OF-FREEDOM NONLINEAR OSCILLATOR

Bendegúz D. BAK[1], Róbert ROCHLITZ[2], Tamás KALMÁR-NAGY[3], Gergely KRISTÓF[4]

[1] Corresponding Author. Department of Fluid Mechanics, Faculty of Mechanical Engineering, Budapest University of Technology and Economics. Bertalan Lajos u. 4 - 6, H-1111 Budapest, Hungary. E-mail: bak.bendeguz@gpk.bme.hu
[2] Department of Fluid Mechanics, Faculty of Mechanical Engineering, Budapest University of Technology and Economics. E-mail: rochlitz.robert.z@gmail.com
[3] Department of Fluid Mechanics, Faculty of Mechanical Engineering, Budapest University of Technology and Economics. E-mail: kalmar.nagy.tamas@gpk.bme.hu
[4] Department of Fluid Mechanics, Faculty of Mechanical Engineering, Budapest University of Technology and Economics. E-mail: kristof.gergely@gpk.bme.hu

ABSTRACT

We study the energy transfer process in a binary tree structured mechanical oscillator that has strongly nonlinear dissipative elements. The masses and spring stiffnesses of the system are tuned to closely match the eigenfrequencies of the oscillator with the eddy frequencies deduced from the characteristic eddy lengths of a turbulent flow. These eddy lengths were obtained from actual measurements of airflow passing through an urban street canyon model carried out in the large wind tunnel of the Theodore von Kármán Wind Tunnel Laboratory. We demonstrate that the model exhibits an energy cascade and compare its features with those of the classical turbulent energy cascade for different types of excitations. We show how the energy is distributed across the different scales of the system. The primary mechanism behind the observed energy transfer is analyzed for different excitation types. We compute wavelet transforms and visualize them on the so-called frequency-energy plot of the system to show the underlying dynamics. The results demonstrate evidence of irreversible energy transfer from the linear part towards the nonlinear dissipative parts of the system through nonlinear beats and fundamental targeted energy transfer.

Keywords: energy cascade, nonlinear dynamics, turbulent flow

NOMENCLATURE

A	[-]	amplitude
E	[-]	total energy
K	[-]	level stiffness
L	[m]	eddy length
M	[-]	level mass
Q	[-]	quality function
a	[-]	parameter for setting the initial energy
c	[-]	damping coefficient
d	[-]	common ratio of geometric series
k	[-]	element stiffness
m	[-]	element mass
n	[-]	number of levels
x	[-]	position
δ	[-]	Kronecker delta
κ	[-]	wavenumber
Ω	[$1/s$]	eddy frequency
ω	[-]	frequency
ρ	[$1/m^3$]	density

Subscripts and Superscripts

i	index of element
j	index of level
$\bar{}$	temporal average
$\hat{}$	spectrum with respect to wavenumber

1. INTRODUCTION

In many engineering applications, there are processes involving energy transfer between a range of different scales. Nowadays an important aspect of this is targeted energy transfer (TET). Kerschen et al. [1] showed that by attaching a nonlinear energy sink (NES) to a linear system, a major portion of the induced energy can be dissipated leading to irreversible targeted energy transfer from the primary system towards the nonlinear dissipative element. The study of the dynamics of systems involving one or multiple NESs has generated tremendous amount of papers. E.g., Gendelman [2] extended the existing methods to systems with non-polynomial nonlinearity, that were originally developed to analyse cubic TET in systems with cubic nonlinearity. Viguié et

al. [3] used passive nonlinear TET to stabilize drill strings, reducing the torsional vibrations arising during operation. Motato et al. [4] showed that the use of NESs in automotive drivelines resulted in redistribution of vibrational energy. In a recent paper Chen et al. [5] demonstrated that parallel-coupled NESs are more efficient at dissipating medium shocks than parallel NESs and perform no worse than a single degree of freedom NES in the whole force range examined.

Targeted energy transfer also arises in turbulent flows. According to Richardson [6], the larger vortical structures that represent the large scales of turbulent flow break up into smaller ones due to their instability, transferring their kinetic energy to smaller and smaller scales, until viscous processes take over. A mathematical description of the energy spectrum of these turbulent scales was given by Kolmogorov [7] for 3D homogenous isotropic turbulence, which characterizes Richardson's energy cascade. In this description, the total energy E is given by

$$E = \int \hat{E}(\kappa) \mathrm{d}\kappa, \tag{1}$$

where $\kappa \sim 1/L$ is the wavenumber associated to the turbulent scale L, $\hat{E}(\kappa)$ is the energy content associated with the scales that have wavenumber κ.

In recent years there have been efforts to reproduce the Kolmogorov spectrum using a mechanistic model of turbulence, consisting of linear oscillators. Kalmár-Nagy and Bak [8] showed that for a well chosen power law describing the stiffnesses of the system, the $\hat{E}(\kappa) \propto \kappa^{-5/3}$ inertial range of the spectrum can be qualitatively obtained from the model.

In this paper a new nonlinear variant of the mechanistic model of Kalmár-Nagy and Bak [8, 9] is studied. The difference between the structure of this nonlinear model variant and the original model is that the dissipative elements are nonlinear energy sinks and they are not attached to a motionless wall. After introducing the chosen parameters of the model and the tools of the analysis in Section 2, the dynamics of the system is analyzed in Section 3 for different types of initial conditions. In Section 4 conclusions are drawn.

2. MECHANISTIC TURBULENCE

2.1. Description of the model

In this paper, a mechanistic model of turbulence is used, which is a $n = 6$ level binary tree of masses connected by springs and dampers as shown in Figure 1. The mass in the top level is connected to a stationary ceiling, and the masses in the bottom level are connected to the previous level by springs with cubic nonlinearity and linear dampers. In general, an element i of level j is connected to the element $\lfloor i/2 \rfloor$ of level $j-1$, and the elements $2i, 2i+1$ of level $j+1$.

The model parameters are considered to be the same across the elements of a level, thus each level j can be characterized with the mass m_j of its elements,

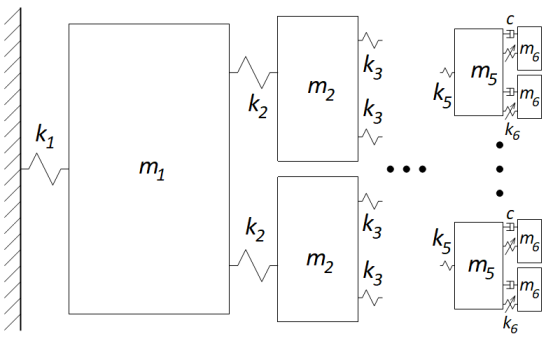

Figure 1. Binary tree of spring connected masses

the stiffness k_j of its springs, and with the damping c in the case of the last level. The equations describing the motion of the i^{th} mass in the j^{th} level:

$$\begin{aligned}
&m_j\ddot{x}_i + k_j x_i + k_{j+1}(x_i - x_{2i}) + \\
&\quad + k_{j+1}(x_i - x_{2i+1}) = 0, \quad \text{if } j = 1, \\
&m_j\ddot{x}_i + k_j(x_i - x_{\lfloor i/2 \rfloor}) + k_{j+1}(x_i - x_{2i}) + \\
&\quad + k_{j+1}(x_i - x_{2i+1}) = 0, \quad \text{if } j \in \{2, 3, 4\}, \\
&m_j\ddot{x}_i + c(\dot{x}_i - \dot{x}_{2i}) + c(\dot{x}_i - \dot{x}_{2i+1}) + \\
&\quad + k_j(x_i - x_{\lfloor i/2 \rfloor}) + k_{j+1}(x_i - x_{2i})^3 + \\
&\quad + k_{j+1}(x_i - x_{2i+1})^3 = 0, \quad \text{if } j = 5, \\
&m_j\ddot{x}_i + c(\dot{x}_i - \dot{x}_{\lfloor i/2 \rfloor}) + k_j(x_i - x_{\lfloor i/2 \rfloor})^3 = 0, \\
&\qquad\qquad \text{if } j = 6
\end{aligned} \tag{2}$$

Throughout this work, Eq. (2) is solved using Wolfram Mathem- atica's built-in numerical differential equation solver (NDSolve). The desired accuracy was set to 8 significant digits. The NDSolve function automatically determines the best numerical scheme for the problem and uses adaptive step size to obtain the required accuracy.

An important quantity is the energy of a given level j that is defined to be the kinetic energy of the masses of the level, and half of the potential energy of the springs connecting to these masses:

$$\begin{aligned}
E_j(t) = &\tfrac{1}{2} m_j \textstyle\sum_{i=2^{j-1}}^{2^j-1} \dot{x}_i(t) + \\
&+ \tfrac{(1+\delta_{1,j})}{4(1+\delta_{n,j})} k_j \textstyle\sum_{i=2^{j-1}}^{2^j-1} \left(x_i(t) - x_{\lfloor i/2 \rfloor}\right)^2 + \\
&+ \tfrac{1}{4(1+\delta_{n-1,j})} k_{j+1} \textstyle\sum_{i=2^j}^{2^{j+1}-1} \left(x_i(t) - x_{\lfloor i/2 \rfloor}\right)^2, \\
&\qquad\qquad \text{for } j \in \{1, \ldots, 6\},
\end{aligned} \tag{3}$$

where δ is the Kronecker delta ($\delta_{i,j} = 1$, if $i = j$ and $\delta_{i,j} = 0$ otherwise). With these, the total energy of the system is

$$E(t) = \sum_{j=1}^{6} E_j(t). \tag{4}$$

The temporal average energy of a level for a time

window $t \in [t_1, t_2]$ is

$$\bar{E}_j = \frac{1}{t_2 - t_1} \int_{t_1}^{t_2} E_j(t) dt \tag{5}$$

A temporal energy spectrum of the system can be interpreted as the level energies scaled by the total energy of the system, i.e.

$$\hat{E}_j(\kappa_j) = \bar{E}_j / \bar{E}, \tag{6}$$

where $\kappa_j = 1/m_j$ is the mass wavenumber. This energy spectrum shows the contribution of each scale m_j to the total energy of the system.

2.2. Model parameters

The masses and the spring stiffnesses were set based on eddy lengths and frequencies of a turbulent flow. These were obtained from measurements of an airflow passing through an urban street canyon model, that was performed in the large wind tunnel of the Theodore von Kármán Wind Tunnel Laboratory. This experiment provided several eddy lengths and frequencies, from which six were selected such that they represent different scales, these are shown in Table 1.

The masses of the elements were directly calculated from the eddy lengths as

$$m_j = \rho L_j^3. \tag{7}$$

The choice of parameter ρ is arbitrary, but in order to obtain masses with the same order of magnitude as in previous works [8, 9], the value of $\rho = 1000\ 1/m^3$ was chosen. Note that due to the model parameters being dimensionless, the unit of ρ was changed to preserve dimensional homogeneity in Eq. (7).

The light damping was prescribed to ensure that the system exhibits strongly nonlinear dynamics, the damping coefficient values were set to

$$c = 0.001. \tag{8}$$

It was found that for significantly higher or lower damping, it is difficult to obtain targeted energy transfer. As examining TET in the system was the goal of the paper, c was chosen such that the oscillator could exhibit this behaviour.

Table 1. Turbulent flow measurements

j	Eddy length, L_j [m]	Eddy frequency, Ω_j [1/s]
1	0.14637	23.208
2	0.12775	53.222
3	0.08710	68.074
4	0.07789	39.060
5	0.03418	84.279
6	0.01502	170.663

The spring stiffnesses were set such that the eigenvalues of the purely linear variant of the model approximately match the eddy frequencies listed in Table 1. In the linear model variant the nonlinear springs are simply replaced by linear springs. In order to obtain the correct spring stiffnesses, one more simplification was employed to reduce computational burden: the binary tree was replaced by a chain of M_j masses connected by linear springs with stiffness K_j, where $M_j = 2^{j-1} m_j$ and $K_j = 2^{j-1} k_j$. This reduced model shown in Figure 2 made the search for the spring stiffness parameters computationally affordable, while it also "preserved" the eigenvalues of the linear binary tree structured oscillator. This means that every eigenvalue of the reduced chain oscillator is an eigenvalue of the binary tree structured oscillator, while obviously the binary tree structured oscillator has additional eigenvalues.

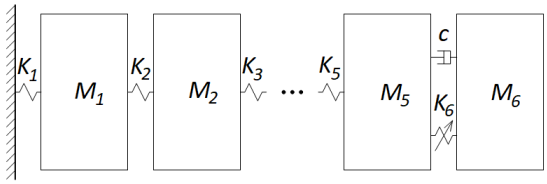

Figure 2. Chain of spring connected masses

The K_j stiffnesses were optimised by searching for the minimum of the quality function

$$Q = \sum_{j=1}^{6} \left| \Omega_j - \Im(\lambda_j) \right| \tag{9}$$

using a simple genetic algorithm, where λ_j are the eigenvalues of the model and $\Im(.)$ denotes the imaginary part function.

The resulting model parameters are shown in Table 2.

Table 2. Model parameters obtained from the turbulence measurements

j	m_j	k_j
1	3.13586	5303.1
2	2.08489	1391.54
3	0.660776	1190.65
4	0.472547	510.463
5	0.0399316	80.9006
6	0.00338852	98.6928

2.3. Frequency-energy plot

A very powerful tool of analysing these nonlinear systems is the frequency-energy plot (FEP). As a nonlinear system has no normal modes or eigenvalues, nonlinear normal modes (NNM) are defined as a time-periodic oscillation of a non-dissipative nonlinear dynamical system [10]. Thus the FEP shows the energy dependence of the frequency corresponding to the NNMs. This plot can be produced by assum-

ing periodic oscillations as

$$x_i(t) = A_i \cos(\omega t). \tag{10}$$

By substituting this expression into Eq. (2), and solving for A_i at $t = 0$, the $A_i(\omega)$ amplitude-frequency functions can be obtained. From these, the total energy-frequency function can be determined from Eqs. (3) to (4). This was done for both the nonlinear binary tree model and the nonlinear reduced model (see Figs. 1 to 2), that are compared in Figure 3. This demonstrates that the dynamics of the reduced model is similar indeed, but its FEP shows that the NNMs of the reduced chain oscillator have a higher energy content for a given frequency in general.

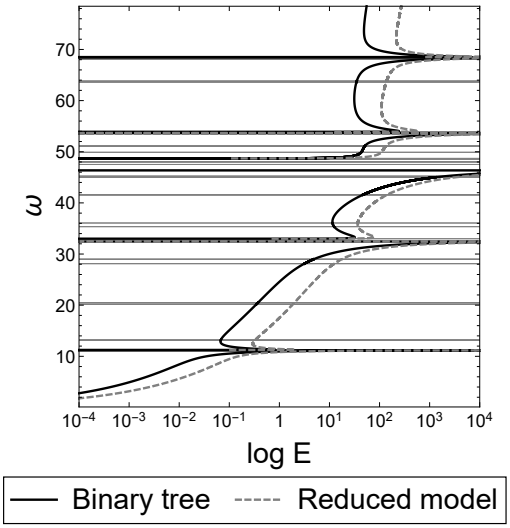

Figure 3. FEPs of the binary tree structured and the chain oscillator

3. SIMULATION RESULTS

The system was investigated with impulsive excitations exclusively, meaning that no forcing was applied. In every examined case, the system was started from equilibrium, i.e.

$$x_i(0) = 0 \quad \forall i \in \{1, \ldots, 63\}. \tag{11}$$

Three types of initial velocities were investigated, the first is nonzero initial conditions in the first five levels. In this case, the initial kinetic energy of different levels follows a geometric sequence, it is equal for elements in the same level, and is zero for the bottom level:

$$\begin{aligned} &\dot{x}_i(0) = \sqrt{\tfrac{ad^j}{m_j}}, \quad i \in \left\{2^{j-1}, \ldots, 2^j - 1\right\}, \\ &\quad j \in \{1, \ldots, 5\}, \\ &\dot{x}_i(0) = 0, \quad i \in \left\{2^{j-1}, \ldots, 2^j - 1\right\}, j = 6, \end{aligned} \tag{12}$$

where the parameter a was used to set the initial total energy of the system. The next type is nonzero initial conditions in a single $j \in \{2, 3, 4\}$ level of the tree, where the initial velocities of the masses in level j follow a geometric sequence:

$$\begin{aligned} &\dot{x}_i(0) = ad^i, \quad i \in \left\{2^{j-1}, \ldots, 2^j - 1\right\}, \\ &\dot{x}_i(0) = 0, \quad i \notin \left\{2^{j-1}, \ldots, 2^j - 1\right\}. \end{aligned} \tag{13}$$

Finally, in the last type the first level was started with an initial velocity of 1, and the elements of the second level with initial velocities of ±1:

$$\begin{aligned} &\dot{x}_1(0) = 1, \\ &\dot{x}_2(0) = \pm 1, \\ &\dot{x}_3(0) = \pm 1. \end{aligned} \tag{14}$$

3.1. Nonzero initial conditions in the first five levels

The system was launched from the initial conditions Eq. (12) for several $E(0)$ initial energy levels and d common ratios. At $t = 1000$, the ratio of the total energy and the initial energy were calculated, the contour plot of this ratio is shown in Figure 4 for the different $E(0)$ and d values. This shows that the behaviour of the system is very sensitive to the initial energy level, as well as the initial energy distribution among the levels of the binary tree.

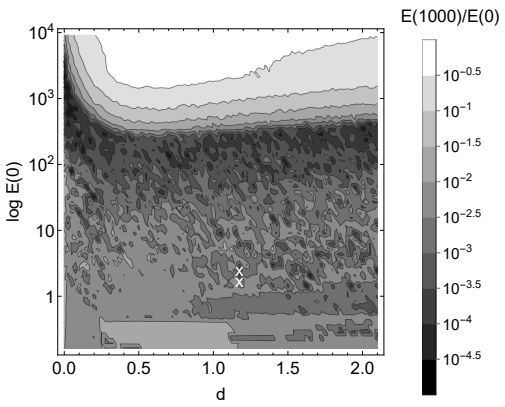

Figure 4. Fraction of the remaining energy as a function of $E(0)$ and d, with initial conditions given in Eq. (12). White x's denote the points used as initial conditions in Eq. (15)

Next the system was examined for two particular sets of initial conditions that are marked by white crosses in Fig. 4. These were chosen such that they are close to each other, but have a significantly different portion of their initial energy remaining at $t = 1000$. In both cases, $d = 1.175$, and the initial energies are:

$$\begin{aligned} E_{(1)}(0) &= 1.728 \\ E_{(2)}(0) &= 2.488 \end{aligned} \tag{15}$$

The fraction of the total energy of the system in the two cases is shown in Figure 5, demonstrating that even for two very similar initial conditions the behaviour of the system is drastically different.

The fraction of the total energy stored in the last level was calculated for the two cases, these are

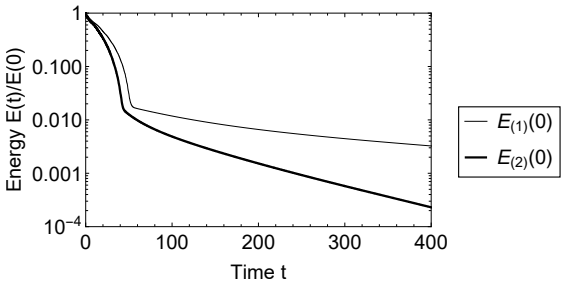

Figure 5. Fraction of the total energy as a function of time, with $d = 1.175$ and initial energy levels from Eq. (15), and initial conditions given in Eq. (12)

shown in Figures 6 and 7. The figures show that for both initial conditions there is a TET, but this occurs around $t = 80$ for $E(0) = E_{(1)}(0)$, in contrast for $t = 100$ for $E(0) = E_2(0)$, and the peak of the energy transfer is also higher for the lower initial energy.

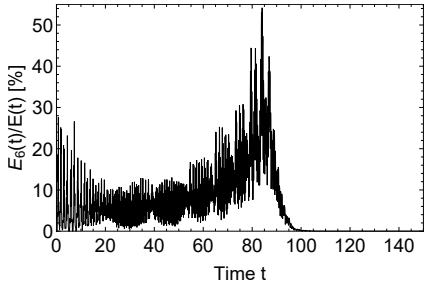

Figure 6. Fraction of the energy stored in the last level as a function of time, $d = 1.175$, $E(0) = E_{(1)}(0)$, with initial conditions given in Eq. (12)

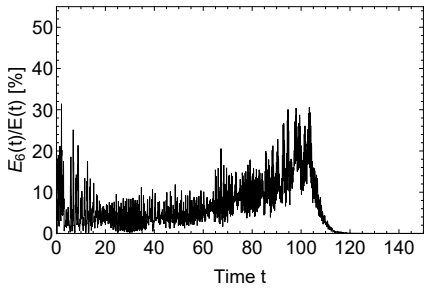

Figure 7. Fraction of the energy stored in the last level as a function of time, $d = 1.175$, $E(0) = E_{(2)}(0)$, with initial conditions given in Eq. (12)

Figures 8 and 9 show the wavelet transform of x_{32}, which shows the frequency of the vibration as the function of its energy content, superimposed onto the FEP for the two initial conditions. In the case of $E(0) = E_{(1)}(0)$, the system follows a backbone curve of the FEP very closely, which indicates that fundamental targeted energy transfer takes place in this case. In case of the higher initial energy level the system does not excite a single NNM, which indicates that the main mechanism of energy transfer is nonlinear beating that allows a more efficient dissipation.

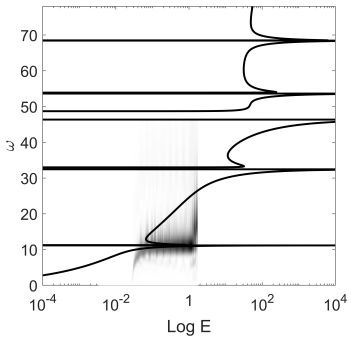

Figure 8. Wavelet transform of x_{32}, with $d = 1.175$, $E(0) = E_{(1)}(0)$, with initial conditions given in Eq. (12)

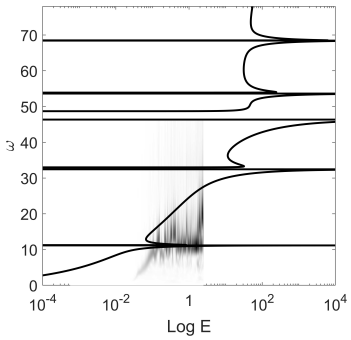

Figure 9. Wavelet transform of x_{32}, with $d = 1.175$, $E(0) = E_{(2)}(0)$, with initial conditions given in Eq. (12)

The temporal average of the energy of the levels was calculated with $t_1 = 0, t_2 = 200$ (see Eq. (5)) and the energy spectra are shown in Figure 10. The main difference between the two results is the energy stored in the last level, which is much lower for the higher initial energy, suggesting that the energy of this level is more efficiently dissipated. Though these spectra do not resemble the Kolmogorov spectrum, their overall trend is qualitatively similar.

3.2. Nonzero initial conditions in a single level

In this case the system was simulated with initial velocities given in Eq. (13) for different $E(0)$ initial energies and d common ratios. Figures 11 to 13 show the fraction of the remaining energy as function of d and $E(0)$ for levels $j \in \{2, 3, 4\}$. Comparing these to Fig. 4, it can be concluded that the behaviour of the system is more sensitive to the distribution of energy among the levels than it is to the distribution among

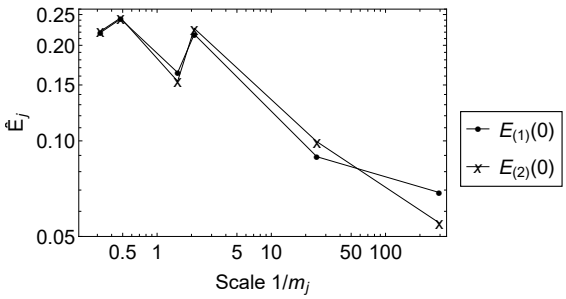

Figure 10. Energy spectrum of the system, with $d = 1.175$ and initial energy levels from Eq. (15), and initial conditions given in Eq. (12)

the masses of the same level. In these cases, the energy dissipation is much more affected by the initial energy.

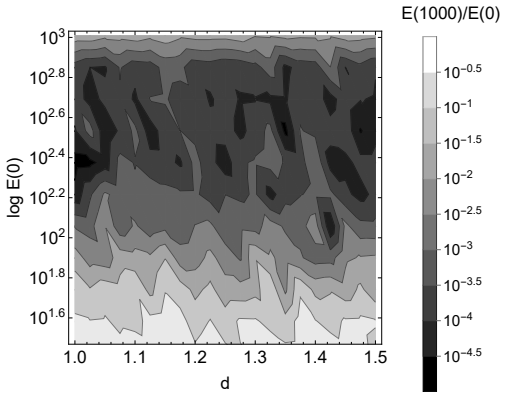

Figure 11. Fraction of the remaining energy as a function of $E(0)$ and d, with initial conditions given in Eq. (13) for level $j = 2$

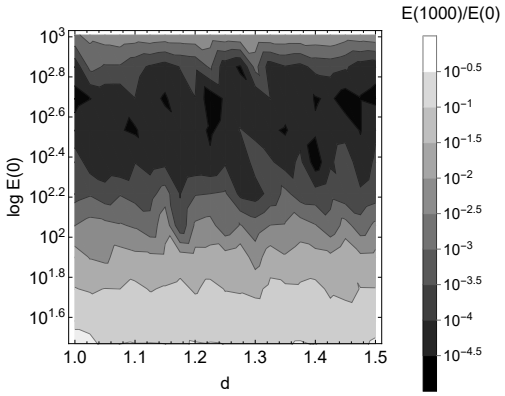

Figure 12. Fraction of the remaining energy as a function of $E(0)$ and d, with initial conditions given in Eq. (13) for level $j = 3$

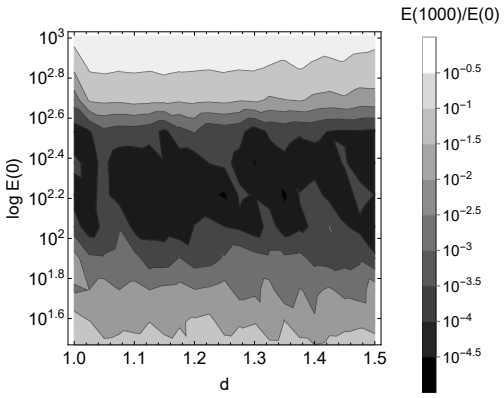

Figure 13. Fraction of the remaining energy as a function of $E(0)$ and d, with initial conditions given in Eq. (13) for level $j = 4$

3.3. Nonzero initial conditions in the first two levels

Finally, the system was examined for the third type of initial conditions specified by Eq. (14). Depending on the sign of $\dot{x}_2(0)$ and $\dot{x}_3(0)$, the system behaves very differently. As the binary tree model is symmetric, there are only 3 cases to be considered:

- $\dot{x}_2(0) = \dot{x}_3(0) = 1$, this will be denoted with $+++$,
- $\dot{x}_2(0) = 1$, $\dot{x}_3(0) = -1$, this will be denoted with $++-$,
- $\dot{x}_2(0) = \dot{x}_3(0) = -1$, this will be denoted with $+--$.

Figure 14 shows the total energy of the system over time for the three set of initial conditions. The total energy dissipation is the highest in the case of $+++$, and the lowest for $+--$.

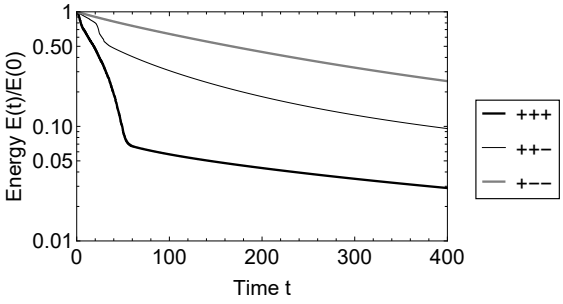

Figure 14. Fraction of the total energy as a function of time, with initial conditions given in Eq. (14

It is clear from Figures 15 to 21 that the energy fraction of the last level is overall the highest for $+++$, and again it is the lowest for $+--$, in which case the peak energy fraction is lower than for the $+++$ and $++-$ initial conditions by a factor of 100.

As there is only significant TET for + + +, it is expected that this initial condition would cause the highest dissipation. Indeed, as there is virtually no energy in the last level for + − −, the behaviour of the system is close to linear.

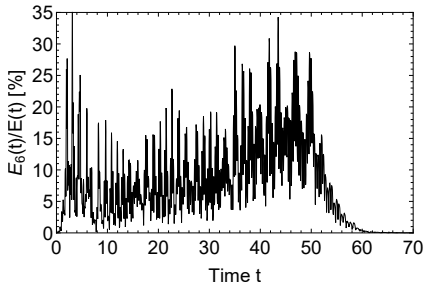

Figure 15. Fraction of the energy stored in the last level as a function of time, with initial conditions given in Eq. (14) and + + +

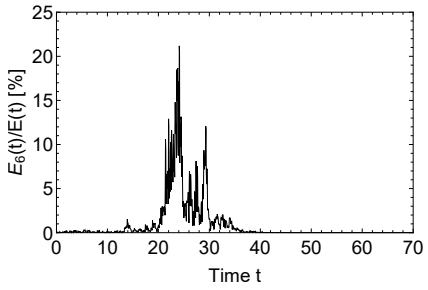

Figure 16. Fraction of the energy stored in the last level as a function of time, with initial conditions given in Eq. (14) and + + −

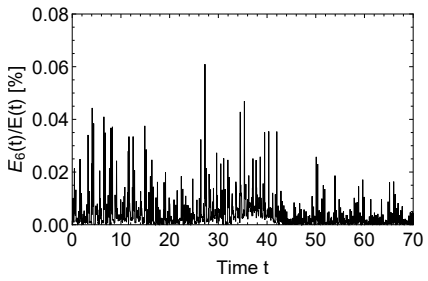

Figure 17. Fraction of the energy stored in the last level as a function of time, with initial conditions given in Eq. (14) and + − −

At last, the wavelet transform of x_{32} is computed for the examined cases, shown in Figures 18 to 20. For the + + + initial condition, the system follows one of the backbone curves, whereas in the other two cases the system remains below the curves throughout the simulation.

Figure 21 shows the energy spectrum of the system in the three cases. The energy stored in the last level was significantly lower for the + + − and + − − initial conditions than for the + + + initial condition. This demonstrates that if the energy of the last level is less, the dissipation is reduced.

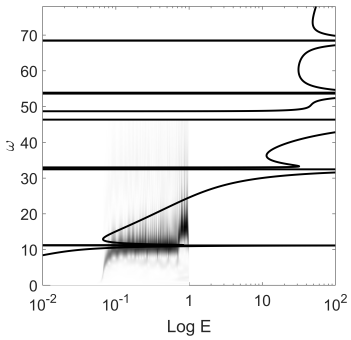

Figure 18. Wavelet transform of x_{32} for initial conditions in Eq. (14) and + + +

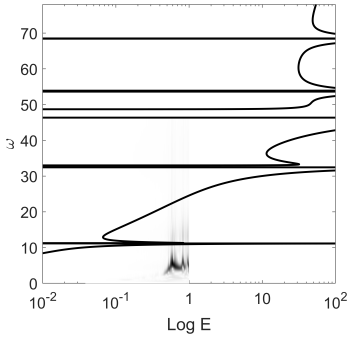

Figure 19. Wavelet transform of x_{32} for initial conditions in Eq. (14) and + + −

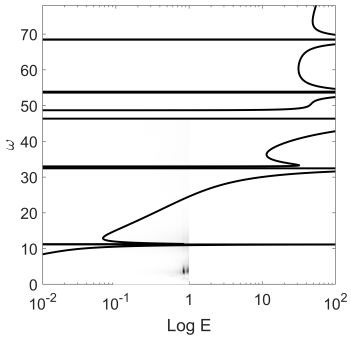

Figure 20. Wavelet transform of x_{32} for initial conditions in Eq. (14) and + − −

4. SUMMARY

The mechanistic model of turbulence was introduced as a binary tree of spring connected masses. The parameters of this model were derived from turbulence measurement data using a reduced model. FEPs were created for the two models to demonstrate their similar behavior. It was found that the reduced model predicts somewhat higher energies for a given frequency of the NNM.

The system was simulated for three types of ini-

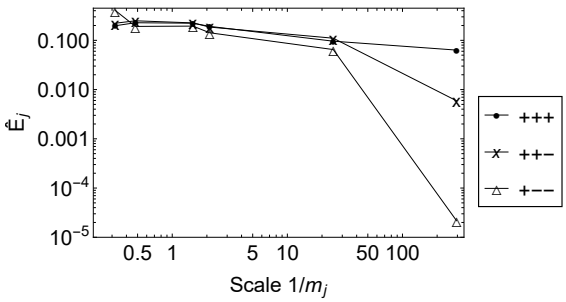

Figure 21. Energy spectrum of the system for initial conditions in Eq. (14)

tial conditions distinguished by the elements with nonzero initial velocities. With nonzero initial velocity in the first 5 levels, the behaviour of the system was found to be very sensitive to both the initial energy and the energy distribution among the levels. It was demonstrated that even a small change in the initial energy content can lead to drastically different dynamical response.

With nonzero initial velocities in a single level, the dynamics of the system were still sensitive to the initial energy, but the energy distribution within the level has little effect on the dissipation of the system.

A case where the only nonzero initial velocities were prescribed for the first two levels was also examined. It was shown that for this initial energy, the dissipation was much more substantial when the three elements started in the same phase in contrast to one or two elements starting in opposite phase to the element of the first level.

The energy spectra of the investigated cases do not resemble the Kolmogorov spectrum, but we also did not expect this from a 6-level system. For now, the purpose of this paper was to present numerical experiments with different initial conditions to give an overview about the dynamics of the system. In future work we intend to investigate the system with much more levels to incorporate a broad scale of masses that will result in a more detailed energy spectrum.

ACKNOWLEDGMENTS

The research reported in this paper and carried out at the Budapest University of Technology and Economics has been supported by the National Research Development and Innovation Fund (TKP2020 National Challenges Subprogram, Grant No. BME-NCS) based on the charter of bolster issued by the National Research Development and Innovation Office under the auspices of the Ministry for Innovation and Technology.

The research reported in this paper is part of project no. BME-NVA-02, implemented with the support provided by the Ministry of Innovation and Technology of Hungary from the National Research, Development and Innovation Fund, financed under the TKP2021 funding scheme.

This work has been supported by the Hungarian National Research, Development and Innovation Fund under contract NKFI K 137726.

REFERENCES

[1] Kerschen, G., Kowtko, J. J., and Mcfarland, D. M. e. a., 2006, "Theoretical and Experimental Study of Multimodal Targeted Energy Transfer in a System of Coupled Oscillators", *Nonlinear Dynamics*, Vol. 47, pp. 285–309.

[2] Gendelman, O. V., 2008, "Targeted energy transfer in systems with non-polynomial nonlinearity", *Journal of Sound and Vibration*, Vol. 315, pp. 732–745.

[3] Viguié, R., Kerschen, G., Golinval, J.-C., McFarland, D. M., Bergman, L. A., F., V. A., and Wouw, N. v. d., 2009, "Using passive nonlinear targeted energy transfer to stabilize drill-string systems", *Mechanical Systems and Signal Processing*, Vol. 23, pp. 148–169.

[4] Motato, E., Haris, A., Theodossiades, S., Mohammadpour, M., Rahnejat, H., Kally, P., Vakakis, A. F., McFarland, D. M., and Bergman, L. A., 2017, "Targeted energy transfer and modal energy redistribution in automotive drivetrains", *Nonlinear Dynamics*, Vol. 87, pp. 169–190.

[5] Chen, J., Zhang, W., Liu, J., and Hu, W., 2021, "Vibration absorption of parallel-coupled nonlinear energy sink under shock and harmonic excitations", *Applied Mathematics and Mechanics (English Edition)*, Vol. 42 (8), pp. 1135–1154.

[6] Richardson, L. F., 1922, *Weather prediction by numerical process*, Cambridge, University Press.

[7] Kolmogorov, A. N., 1941, "The local structure of turbulence in incompressible viscous fluid for very large Reynolds numbers", *Dokl Akad Nauk SSSR*, Vol. 30, pp. 301–305.

[8] Kalmár-Nagy, T., and Bak, B. D., 2019, "An intriguing analogy of Kolmogorov's scaling law in hierarchical mass-spring-damper model", *Nonlinear Dynamics*, Vol. 95.

[9] Bak, B. D., and Kalmár-Nagy, T., 2019, "Energy Cascade in a Nonlinear Mechanistic Model of Turbulence", *Technische Mechanik*, Vol. 39, pp. 64–71.

[10] Vakakis, A. F., Gendelman, O. V., Bergman, L. A., McFarland, D. M., Kerschen, G., and Lee, Y. S., 2008, *Nonlinear Targeted Energy Transfer in Mechanical and Structural Systems*, Springer.